EMERGING PERSPECTIVES ON MERCURY'S INTERNAL STRUCTURE FROM MESSENGER FLYBY OBSERVATIONS AND GEOPHYSICAL MODELING. Maria T. Zuber[1], David E. Smith[1], Roger J. Phillips[2], Sean C. Solomon[3], Gregory A. Neumann[4], Frank G. Lemoine[4], Stanton J. Peale[5], Jean-Luc Margot[6], Steven A. Hauck, II[7], James W. Head[8], Catherine L. Johnson[9], Michael E. Purucker[4], Jürgen Oberst[10], Grant T. Farmer[1], Jiangning Lu[1], Youshun Sun[1], M. Nafi Toksöz[1], Olivier S. Barnouin[11], Mark E. Perry[11], Dipak K. Srinivasan[11], Mark H. Torrence[12], [1]Massachusetts Institute of Technology, Cambridge, MA 02129 (zuber@mit.edu); [2]Southwest Research Institute, Boulder, CO 80302; [3]Carnegie Institution of Washington, Washington, DC 20015; [4]NASA Goddard Space Flight Center, Greenbelt, MD 20771; [5]University of California, Santa Barbara, CA 93106; [6]University of California, Los Angeles, CA 90095; [7]Case Western Reserve University, Cleveland, OH 44106; [8]Brown University, Providence, RI 02912; [9]University of British Columbia, Vancouver, BC, Canada V6T 1Z4; [10]DLR, Berlin, Germany; [11]Johns Hopkins University Applied Physics Laboratory, Laurel, MD 20723; [12]SGT, Inc., 7701 Greenbelt Rd., Greenbelt, MD 20770.

Introduction: New observations by the MESSENGER spacecraft during its three flybys of Mercury [1] have revealed that the innermost planet preserves a geological record of extended interior activity [2]. Distributed and impact-basin-related tectonics [3-5] and abundant volcanism [6-7] point to active mantle and lithospheric dynamics throughout much of the planet's history [cf. 8-10]. Study of the current internal structure and past plausible structures provide constraints on Mercury's internal dynamics over time that can be linked to the surface record. Geophysical observations from MESSENGER coupled with modeling are contributing to improving understanding of Mercury's interior.

Constraints on Core State: Mercury has long been known to be unique among terrestrial planets because of its relatively large mass in comparison to its size, implying a predominantly iron core about ¾ the planetary radius. Observations from the MESSENGER Magnetometer complement and enhance understanding from previous observations provided by Mariner 10 flybys [11]. The MESSENGER data verify that Mercury has a present-day magnetic field [12, 13] with a dipole that aligns closely with the spin axis [14]. Such a magnetic field geometry is likely indicative of a core dynamo within a partially molten liquid outer core [15], which implies currently active interior dynamics.

Constraints on the early core state have been explored from modeling of seismic waves associated with the Caloris impact to explain hilly and lineated terrain at the basin's antipode [16]. Recent modeling [17] shows that there is considerable sensitivity regarding the nature of focusing to the source depth of the impact, with shallow peak stresses (~20 km) dominated by surface waves and deep peak stresses (~100 km) dominated by body waves. Surface-wave-dominated antipodal disruption places no constraint on core state. For body waves effects on the seismic responses from the internal state and the source function are coupled. For fluid core models antipodal disruption at the antipode may have been accompanied by extensive shallow plastic deformation.

Internal Structure from Equatorial Altimetry and Gravity: Data from the Mercury Laser Altimeter (MLA) [18] provided new information on the equatorial shape of Mercury [19], and Doppler tracking [20] of the spacecraft through the flybys provided new data on the planet's gravity field [21]. MLA passes collected during MESSENGER flybys 1 and 2, shown in Fig. 1, were on opposite hemispheres of the planet and spanned collectively 41% of Mercury's equatorial circumference. The mean elevation of topography observed during flyby 1, in the longitude range 0°-90°E, is greater than that of flyby 2 in the longitude range 180-270°E, indicating an offset between center of mass (COM) and center of figure (COF) having a magnitude and phase in general agreement with topography determined by Earth-based radar [22].

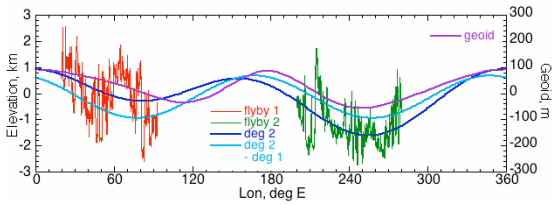

Fig. 1. MLA elevations and coverage for flybys 1 and 2. Elevations are with respect to a sphere of radius 2440 km [17]. Also shown is a spherical harmonic degree-2 fit to the altimetry (in dark blue) and the fit with the degree-1 terms associated with the COM/COF offset removed (in light blue) for comparison with the geoid, which does not contain these terms. The geoid is shown in purple.

Both MLA profiles are characterized by slopes of ~0.015° downward to the east, which is consistent with a long-wavelength equatorial shape defined by axes $a > b$, where a and b are the semi-major and semi-minor axes of the best-fitting ellipse. The Doppler tracking data show sensitivity to the gravitational structure of Mercury. The equatorial ellipticity of the gravitational field, C_{22}, given in Table 2, is well determined and

correlates with the equatorial shape. The S_{22} coefficient is ~0, as would be expected if Mercury's coordinate system is aligned along its principal axes of inertia. The recovered value of the polar flattening of the gravitational potential, C_{20}, is considerably lower in magnitude than obtained from Mariner 10 tracking, a result that is problematic for internal structure models [cf. 23]. This parameter is not as well constrained as the equatorial ellipticity because the flyby trajectories were nearly in the planet's equatorial plane.

	HgM001 4x4 solution	4x4 σ
GM	22031.80	0.08
C_{20}	-0.857	1.8
C_{22}	1.258	0.7
S_{22}	-0.043	0.9

Table 1. Values of *GM*, spherical harmonic solutions and associated standard deviations (σ) to degree and order 2. For HgM001, C_{21} and S_{21} were set to zero and not estimated. Units: *GM*, σ_{GM} are km^3 s^{-2}; coefficients and σ are x10^{-5}.

Constraints on Crustal and Lithosphere Thickness: For a range of assumptions on degree of compensation and crustal and mantle densities, the allowable crustal thickness is consistent with the upper limit of 140 km estimated from the inferred depth of faulting beneath lobate scarps and an assumed ductile flow law for crustal material [24]. This crustal thickness estimate satisfies a subsolidus constraint on the lowest-most crust (T_m < 1800 K). A lower T_m (1400-1600 K), gives a 80-100 km upper bound. The MESSENGER value of C_{22} has allowed an improved estimate of the ratio of the polar moment of inertia of the mantle and crust to the full polar moment (C_m/C), a refinement that strengthens the conclusion that Mercury has at present a fluid outer core.

If the mean crustal thickness is small relative to the planetary radius, then from the geometric description of equatorial shape, a simple crustal degree-1 thickness difference does not explain the gravity and shape, and additional investigation into implications for internal structure is warranted.

However, a simple mass balance is not a good approximation for compensation of the shape because membrane stresses provide significant support of topography at degree 2 [25]. The degree of compensation for flexural and membrane support is a function of ρ_c and mantle density, ρ_m; Young's modulus, E, and Poisson's ratio, ν; and the effective elastic thickness, T_e.

The gravity constraint, C_{22}, produces a spectrum of solutions ranging from an upper bound on crustal thickness to an upper bound on elastic thickness, with the actual estimated thickness depending, as shown in Fig. 2, on the densities and elastic parameters. With these parameters, the gravity result produces a crustal thickness less than the upper bound of [24]. Stronger constraints on crustal density that should be forthcoming from the MESSENGER mission orbital phase will help refine this solution family.

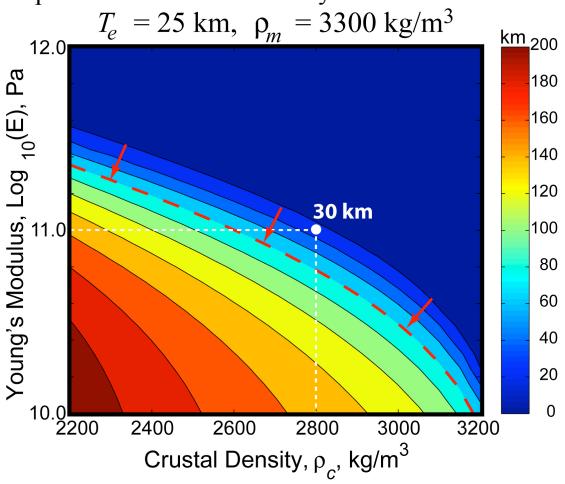

Fig. 2. Solution space for E and ρ_C, using estimated T_e value from [24]. The blue area, which cannot satisfy the C_{22} constraint, is excluded, the white dashed lines are the parameter values used by [24], and the red dashed line is the upper bound on crustal thickness [24] for a mantle temperature of 1400 K.

References: [1] Solomon S. C. et al. (2007) *Space Sci. Rev., 131,* 3-39. [2] Solomon S. C. et al. (2008) *Science, 321,* 59-62. [3] Watters T. R. et al. (2009) *EPSL, 285*, 283-296. [4] Watters T. R. et al. (2009) *EPSL, 285*, 309-319. [5] Watters T. R. et al. (2009) *Science, 324*, 618-621. [6] Head J. W. et al. (2008) *Science, 321*, 69-72. [7] Head J. W. et al. (2009) *EPSL, 285*, 227-242. [8] Hauck S. A. II et al. (2004) *EPSL, 22,* 713-728. [9] Zuber M. T. et al. (2007) *Space Sci. Rev., 131*, 105-132 [10] Zuber M. T. et al. (2009) *Icarus*, submitted. [11] Ness N. F. et al. (1975) *JGR, 80*, 2708-2716. [12] Anderson B. J. et al. (2008) *Science, 321*, 82-85. [13] Uno H. et al. (2009) *EPSL, 285*, 328-339. [14] Anderson B. J. et al. *Space Sci. Rev.,* in press. [15] Margot J. L. et al. (2007) *Science, 316*, 710-714. [16] Melosh H. J. and McKinnon W. B. (1988) in *Mercury,* ed. F. Vilas, C. R. Chapman, M. S. Matthews, Univ. Ariz. Press, Tucson, pp. 374-400. [17] Lu J. et al. (2009) *LPS, 41*, this issue. [18] Cavanaugh J. F. et al. (2007) *Space Sci. Rev., 131,* 451-480. [19] Zuber M. T. et al. (2008) *Science, 321,* 77-79. [20] Srinivasan D. K. et al. (2007) *Space Sci. Rev., 131*, 557-571. [21] Smith D. E. et al. (2009) *Icarus*, submitted. [22] Anderson J. D. et al. (1996) *Icarus, 124*, 590-697. [23] Peale S. J. et al. (2002) *Meteorit. Planet. Sci., 37*, 1269-1283. [24] Nimmo F. and Watters T. R. (2004) *GRL, 31,* doi:10.1029/2003GL018847. [25] Turcotte D. L. (1981) *JGR, 86,* 3952-3959.